AJNR

Arteriovenous shunt measurement during endovascular therapy for cerebrospinal lesions.

L Mariani, A R Haldemann and G Schroth

This information is current as of April 19, 2024.

Arteriovenous Shunt Measurement during Endovascular Therapy for Cerebrospinal Lesions

Luigi Mariani, Andreas R. Haldemann, and Gerhard Schroth

PURPOSE: To determine (*a*) whether superselective angioscintigraphy with technetium-99m macroaggregated albumin (^{99m}Tc-MAA) can be used for the evaluation of arteriovenous shunting in tumors and vascular malformations of the head and spine and (*b*) whether the amount of microparticles shunted is related to diagnosis, lesion size, or angiographic pattern. **METHODS:** Particles of ^{99m}Tc-MAA with a calibrated diameter of 25 to 50 μm were delivered intraarterially in feeders of head and spine tumors and vascular malformations in 38 patients. The first estimation of the proportion of particles reaching the lungs was made on-line in the angiography suite using a hand-held lead-shielded detector. Evaluation of the intralesional shunt (pulmonary shunt index, or PSI) was derived from quantitative gamma camera recordings of tumoral and pulmonary activity after the embolization procedure was complete. **RESULTS:** The PSI value ranged from 48% to 100% for vascular malformations and vascular tumors (n = 11), 82% to 95% for juvenile angiofibromas (n = 4), 63% to 70% for high-grade gliomas (n = 2), 0% to 50% for renal cell carcinoma metastases (n = 4), 0% to 86% for meningiomas (n = 11), and 0% to 36% for paragangliomas (n = 6). Angiographically, the presence of visible arteriovenous channels was predictive of a high PSI. In contrast, the presence of early venous drainage was associated with a wide PSI range. **CONCLUSION:** Superselective ^{99m}Tc-MAA angioscintigraphy of tumors and vascular malformations of the head and spine is a valuable method for quantifying an intralesional arteriovenous shunt before embolization.

Index terms: Arteriovenous malformations, embolization; Interventional materials, embolic agents; Radionuclide imaging; Technetium

Therapeutic endovascular embolization refers to the occlusion of a vessel territory by the selective introduction of embolic agents into the arteriocapillary bed of the lesion. To obtain optimal devascularization, it is essential to deposit the embolic agents as deeply as possible into the tumor or vascular malformation. Complete devascularization of vascular malformations as well as of highly vascularized tumors demands that precapillaries, capillaries, and even the proximal parts of the draining veins are occluded. However, passage of embolic material to normal intracranial arteries (1–3) and passage to the venous system, especially during chemoembolization and radioembolization of malignant tumors, must be avoided.

Polyvinyl alcohol (PVA) microparticles of different sizes are routinely used for preoperative embolization of craniocerebral and spinal lesions. Microspheres are currently being investigated for mechanical embolization (4, 5) or as vehicles for the intraarterial selective delivery of chemotherapeutics or radionuclides in the treatment of cancer (6–9). To achieve effective and safe embolization, it is important to know which would be the smallest particle completely trapped in the capillary bed of a given lesion. This information can be partially ascertained by injecting the embolic agents under fluoroscopic control.

The lungs, being the first organ downstream from the point of injection, will retain any embolic material passing through the lesion. Thus,

measuring the extent of pulmonary trapping for a given particle size will reflect the degree of arteriovenous shunting in the catheterized tissue, as has been shown with tumors in other locations (9–12). The technical improvements in catheterization techniques and the recent development of microcatheters with variable stiffness now permit selective injection in vessels with a luminal diameter as small as 1 to 2 mm. This capability enables the interventional neuroradiologist to study intralesional shunting safely between dangerous arterioarterial anastomoses.

To measure intralesional arteriovenous microparticle shunting, we prospectively performed superselective angioscintigraphy with technetium-99m macroaggregated albumin (^{99m}Tc-MAA) before embolization in patients with tumors and vascular malformations of the head and spine.

Patients and Methods

Patient Population

Thirty-eight patients undergoing presurgical angiography and embolization for tumors and vascular malformations of the head, neck, and spine were entered into the study (Table). Pretherapeutic and posttherapeutic imaging consisted of multiplanar high-field-strength magnetic resonance (MR) imaging, which normally included contrast-enhanced T1-weighted images, and/or high-resolution computed tomography (CT) before and after embolization. The project was approved by the local ethics commission, and patients gave informed consent to participate in the study.

Angiography, ^{99m}Tc-MAA Angioscintigraphy, and Embolization

The following steps were successively undertaken on the day of the procedure:

1) A diagnostic angiographic workup was performed as the first step, including selective and superselective functional neuroangiography to identify the type, number, and geometry of the feeding arteries and to determine the angioarchitecture of the lesion. The procedure was usually performed with local anesthetic administered through the femoral artery using a 4.5F to 5.5F catheter, which allows catheterization of individual feeding arteries in head and neck lesions as well as insertion of a microcatheter for superselective angiography and embolization. A dedicated neurointerventional system, equipped with the possibilities of biplane fluoroscopy, road mapping, and digital subtraction angiography (DSA) (matrix, 1024 × 1024), was used.

2) Superselective catheterization of the distal portion of the feeding arteries of the lesion was performed with a

microcatheter, usually a Tracker 18 or 10 (Target Therapeutics, Fremont, Calif).

3) Following DSA documentation of the superselective catheterization and of the position of the tip of the microcatheter, we slowly injected approximately 170 MBq of freshly prepared ^{99m}Tc-MAA particles (CIS Biointernational, Gif sur Yvette, France) under fluoroscopic control. Ninety-five percent of the ^{99m}Tc-MAA particles had a diameter ranging from 25 to 50 μm. None of the particles was larger than 100 μm or smaller than 10 μm, according to the manufacturer. These particles are known to be trapped in the capillary bed of the lungs following peripheral intravenous injection, and they are used routinely at our hospital in pulmonary perfusion studies (13).

4) With the microcatheter in place, we measured the maximum gamma-ray emission (maximum, 3000 cps) over the lesion and over the right lung (anterior and posterior projections) using a portable, lead-shielded probe (235 Isotope Localisation Monitor, Pitman Instruments, Weybridge, England).

5) The tumor selectivity ratio (TSR) was calculated in the angiography suite as TSR = cps over the tumor/cps over the right lung.

6) Embolization of the lesion was performed, usually with glue or PVA particles, mostly in the range of 100 to 500 μm (Contour, Interventional Therapeutics Corp, San Francisco, Calif). Particles as small as 45 μm were used if no radioactivity was detected over the lungs by the former measurement.

7) The procedure was completed by angiography using the original position of the guiding catheter and biplane projections as described in step 1 to control and document the effect of embolization.

8) After removal of the femoral catheter or sheath and femoral compression, the patient was transported to the department of nuclear medicine for scintigraphy of the lesion and the thorax with a gamma camera (Gamma Diagnost, Philips AG, Eindhofen, the Netherlands) attached to a computer system. Two hundred thousand to 300 000 counts were recorded from the image with maximal activity. An identical recording time was used to make the other images.

9) With a dedicated computer program, after correcting the background and considering carefully drawn regions of interest as described elsewhere (11), we calculated the pulmonary shunt index (PSI) as PSI = (activity over the lungs/activity over both tumor and lungs) × 100.

Histologic Diagnosis, Angiographic Characteristics, and Size of the Lesions

Histologic diagnosis was obtained in all patients, except for those with vascular malformations. The lesions were subdivided into three types according to their appearance in the angiographic workup: type 1, visible arteriovenous channels; type 2, presence of early venous drainage, strong parenchymal blush, no visible arteriovenous channels; type 3, presence of a strong parenchymal blush but no visible arteriovenous channels or early venous drainage.

Characteristics of the study population and results of arteriovenous shunt measurements

Case	Age, y/Sex	Diagnosis	Location	Feeder	Maximal Diameter, mm	Angiographic Type	Pulmonary Shunt Index, %
1	23/M	Intramedullary AVM	Vertebral level T-11	A intercostalis	10 (nidus)	1	99
2	38/F	Cerebral AVM	Frontal	A cerebri media	40 (nidus)	1	100
3	37/F	Cerebral AVM	Parietal	A gyri angularis	20 (nidus)	1	99
4	59/M	Dural angioma	Sinus transversus	C-1 anastomosis	NA	1	60
5	58/F	Dural angioma	Sinus rectus	A meningea media	NA	1	48
6	72/M	Dural angioma	Sinus transversus	A meningea media	NA	1	76
7	73/F	Dural angioma	Sinus petrosus	A pharyngea ascendens	NA	1	99
8	53/F	Hemangioma	Vertebral body L-4	A lumbalis	30	3	42
9	52/F	Hemangioblastoma	Cerebellum	A meningea media	35	2	61
10	12/F	Arteriovenous angioma	Cheek	A fascialis	50	2	95
11	61/M	Capillary venous angioma	Cheek	A temporalis superficialis	90	2	90
12	69/F	Glomus tumor	Glomus vagale	A pharyngea ascendens	45	2	18
13	54/F	Glomus tumor	Glomus jugulare	A pharyngea ascendens	30	2	0
14	56/F	Glomus tumor	Glomus tympanicum	A pharyngea ascendens	10	2	0
15	78/F	Glomus tumor	Glomus tympanicum	A pharyngea ascendens	10	2	36
16	77/F	Glomus tumor	Glomus caroticum	A pharyngea ascendens	5	2	16
17	58/M	Glomus tumor	Glomus caroticum	A pharyngea ascendens	5	2	3
18	15/M	Juvenile angiofibroma	Nasopharynx	A sphenopalatina	30	2	82
19	17/M	Juvenile angiofibroma	Nasopharynx	A sphenopalatina	70	2	94
20	15/M	Juvenile angiofibroma	Nasopharynx	A pharyngea ascendens	80	2	89
21	16/M	Juvenile angiofibroma	Nasopharynx	A maxillaris	30	2	95
22	57/M	Glioblastoma multiforme	Frontal lobe	A praefrontalis	55	2	70
23	30/M	Anaplastic oligodendroglioma	Frontal lobe	A meningea media	45	2	63
24	50/F	Meningioma	Posterior fossa	A occipitalis	50	†	0
25	68/F	Meningioma	Frontal convexity	A meningea accessoria	50	2	0
26	43/F	Meningioma	Sphenoid wing	A meningea media	60	2	86
27	68/F	Meningioma	Os petrosus	A meningea media	20	2	3
28	50/F	Meningioma	Parasagittal	A meningea media	25	3	5
29	73/F	Meningioma	Frontobasal	A meningea media	60	3	1
30	57/M	Meningioma	Tentorium cerebelli	A meningea media	25	3	0
31	66/F	Meningioma	Frontobasal	A meningea media	30	3	0
32	57/F	Meningioma	Occipital convexity	A occipitalis	80	3	5
33	67/M	Meningioma	Frontal convexity	A meningea media	4	2	27
34	27/M	Meningeal sarcoma	Parasagittal	A meningea media	35	2	0
35	30/F	Metastasis, renal cell carcinoma	Vertebral body L-4	A lumbalis	35	2	0
36	68/F	Metastasis, renal cell carcinoma	Vertebral body C-5	A cervicalis ascendens	23	2	0
37	62/M	Metastasis, renal cell carcinoma	Sacrum	A sacralis lateralis	70	3	50
38	53/M	Metastasis, renal cell carcinoma	Sinus maxillaris	A maxillaris	60	†	14

Note.—AVM indicates arteriovenous malformation; NA, not applicable.

* Lost to evaluation.

† See "Methods" section of text.

The maximal diameter of the lesion was measured on CT or MR studies except in those patients with dural arteriovenous fistulas (AVFs).

Results

Patient data, histologic diagnosis, location of the lesion, catheterized arterial feeder, maximal lesion diameter, angiographic type, and PSI are shown in the Table. Illustrative cases are shown in Figures 1 through 4.
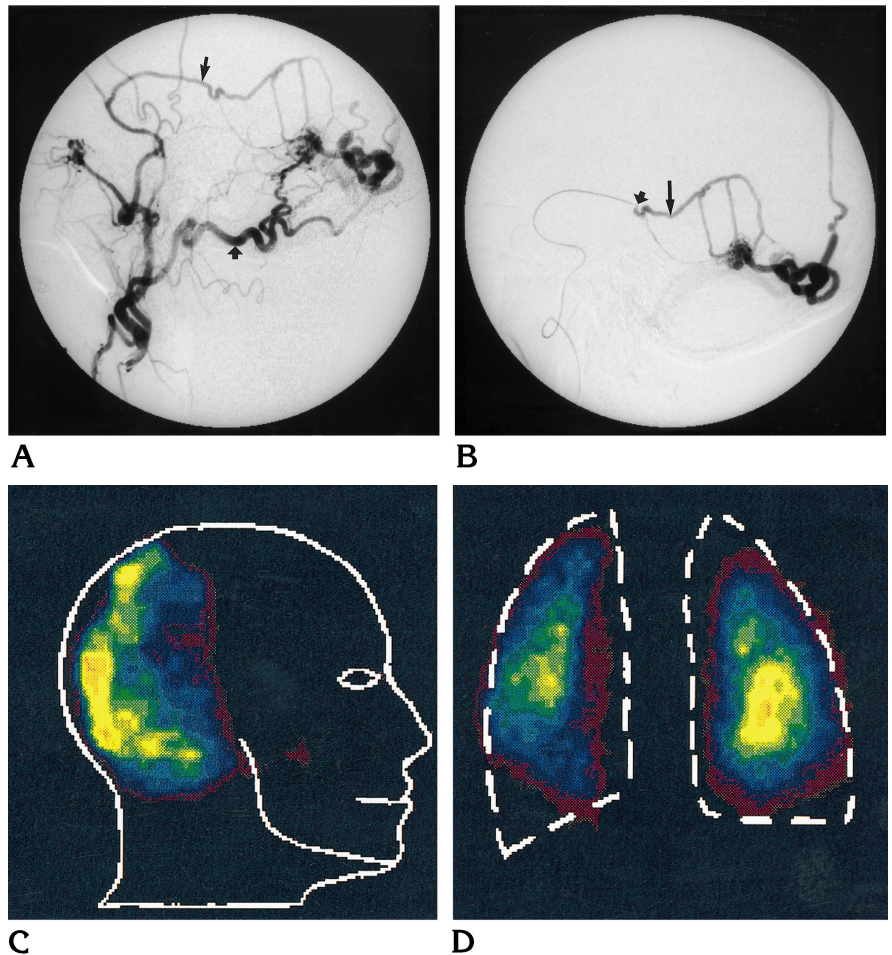
No adverse reactions were observed after intraarterial injection of ^{99m}Tc-MAA. On-line measurement of gamma-ray emission with the hand-held detector was possible in 24 of the 38 patients. There was a positive correlation between increasing TSR and decreasing PSI ($r =$

Fig 1. Patient 6: dural fistula.

A, External carotid angiogram shows branches of the occipital (*short arrow*) and middle meningeal (*long arrow*) arteries feeding a dural AVF draining into a large vein in the region of the transverse sinus.

B, Superselective angiogram shows middle meningeal artery (*long arrow*) supplying the dural AVF before embolization. *Short arrow* indicates the position of the catheter tip, from which ^{99m}Tc-MAA angioscintigraphy and glue embolization were performed.

C and *D*, Scintigrams of the head (*C*) and lungs (*D*) show intense pulmonary activity as a consequence of the intralesional shunt.

.86), as shown in Figure 5. A TSR of more than 10 was always associated with a PSI of less than 30%. In one patient with an intramedullary angioma, the measurement was not reliable because of anatomic proximity to the lungs. Data from the hand-held detector were not precise in the remaining cases because the activity exceeded the capacity of the hand-held monitor (3000 cps).

Lesion Type and PSI (Fig 6)

A high PSI (mean, 79%; range, 42 to 100) was found in vascular lesions (three arteriovenous malformations [AVMs], four dural AVFs, two facial angiomas, one vertebral hemangioma, and one hemangioblastoma). For the remaining 27 solid tumors, a wide range of PSI was found. Juvenile angiofibromas had a mean PSI of 90% (range, 82% to 95%). High-grade gliomas, one anaplastic oligodendroglioma, and one glioblastoma, had a PSI of 63% and 70%, respectively (mean, 67%). Patients with

metastases of renal cell carcinoma showed a PSI of 0%, 0%, 14%, and 50% (mean, 16%). Glomus tumors had a PSI of 0%, 0%, 3%, 16%, 18%, and 36% (mean, 12%). PSIs were especially low in meningiomas (mean, 12%); however, in two cases, we found a PSI of 27% (mixed fibroblastic and meningothelial type) and 86% (meningothelial type).

Lesion Size and PSI

Overall, there was no significant correlation between the maximal lesion diameter and the PSI. The histologic subgroups were too small to allow statistical analysis. However, even considering the largest subgroup of meningiomas (n = 11), no correlation was found ($P = .1752$).

Angiographic Characteristics and PSI

Seven lesions had visible arteriovenous channels detected during the angiographic workup (type 1); all of them were AVMs or dural AVFs.
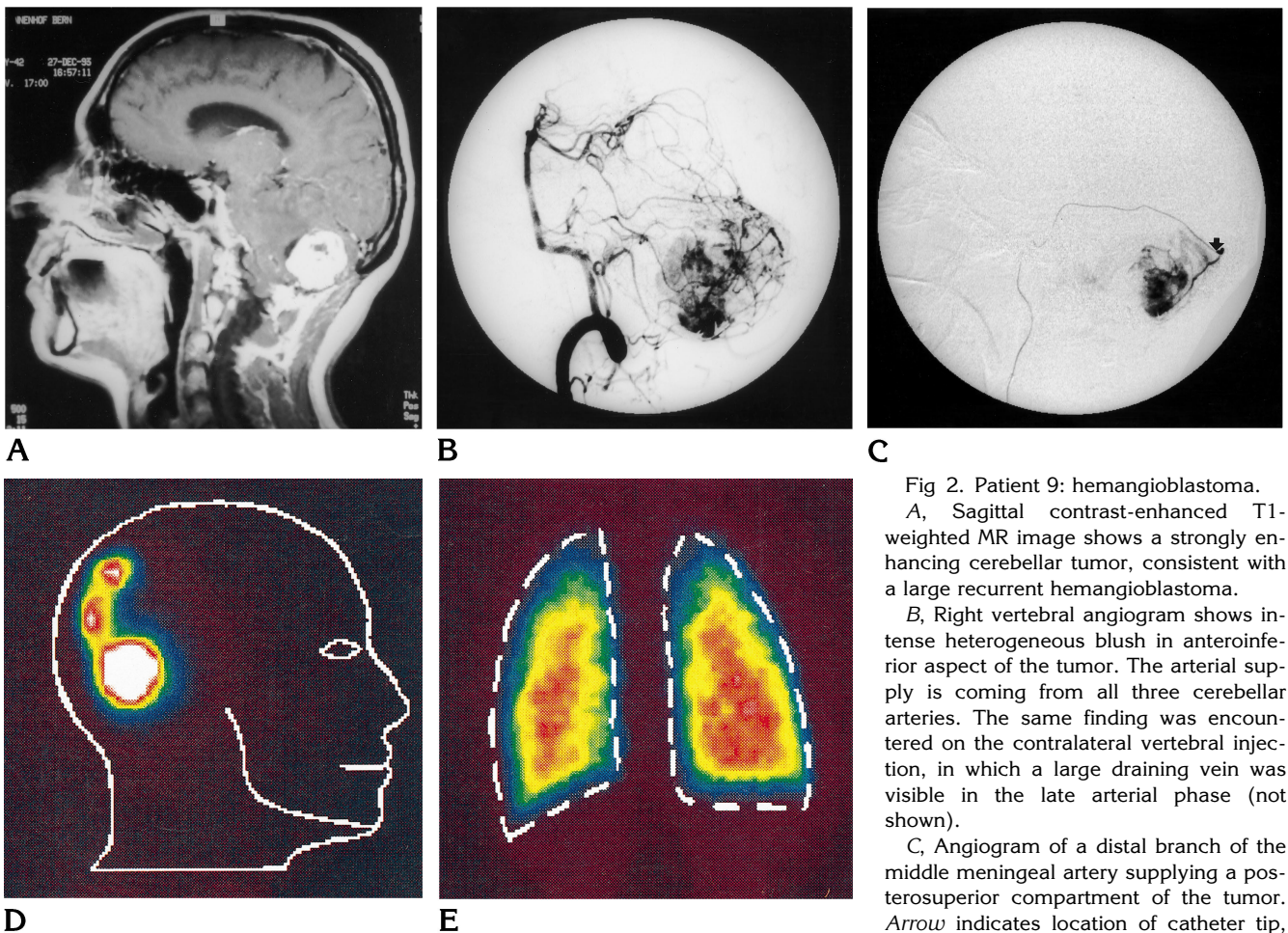
Fig 2. Patient 9: hemangioblastoma.

A, Sagittal contrast-enhanced T1-weighted MR image shows a strongly enhancing cerebellar tumor, consistent with a large recurrent hemangioblastoma.

B, Right vertebral angiogram shows intense heterogeneous blush in anteroinferior aspect of the tumor. The arterial supply is coming from all three cerebellar arteries. The same finding was encountered on the contralateral vertebral injection, in which a large draining vein was visible in the late arterial phase (not shown).

C, Angiogram of a distal branch of the middle meningeal artery supplying a posterosuperior compartment of the tumor. *Arrow* indicates location of catheter tip, from where ^{99m}Tc-MAA was injected for scintigraphy just before embolization with particles (150 to 250 µm).

D and *E,* Scintigrams of the head (*D*) and lungs (*E*) show intense pulmonary activity as a consequence of the intralesional shunt.

Twenty-two additional lesions showed an early venous drainage and a strong parenchymal blush (type 2): six glomus tumors, four angiofibromas, two high-grade gliomas, two facial angiomas (one capillary venous angioma and one arteriovenous angioma), one hemangioblastoma, five meningiomas, and two renal cell carcinoma metastases. Seven lesions showed a strong parenchymal blush without visible arteriovenous channels or early venous drainage (type 3): five meningiomas, one vertebral hemangioma, and one renal cell carcinoma metastasis.

Mean PSIs were 80%, 42%, and 8% in angiographic type 1 (range, 60% to 100%, n = 7), type 2 (range, 0% to 95%, n = 22), and type 3 (range, 1% to 50%, n = 7), respectively. Standard deviations were very high (23%, 38%, and 17%, respectively), especially for type 2.

The absence of early venous drainage (type 3) was invariably associated with a PSI of less than 50%. However, lesions with early venous drainage had PSIs ranging from 0% to 100%. In particular, glomus tumors and juvenile angiofibromas, which share the same angiographic characteristics, had strikingly different PSIs, as shown above.

Discussion

Knowing the amount of intralesional arteriovenous shunting for a given particle size in a given lesion could help in the choice of embolic agents and in the optimization of mechanical embolization, radioembolization (14), and chemoembolization. To date, evaluation of intralesional shunting is based primarily on angiographic characteristics. With short injections of contrast material, a bolus can be followed through blood vessels of the lesion (bolus tracking), and the transit velocity can be compared with that of the adjacent normal parenchyma.

Faster circulation through the lesion with

A

B

C
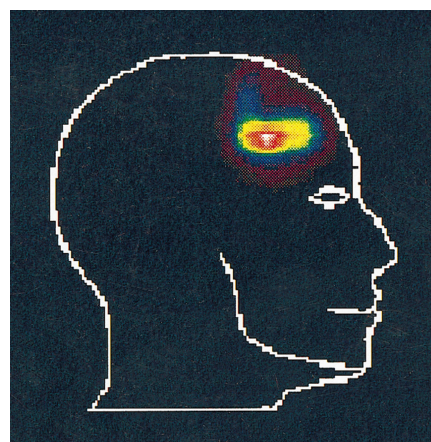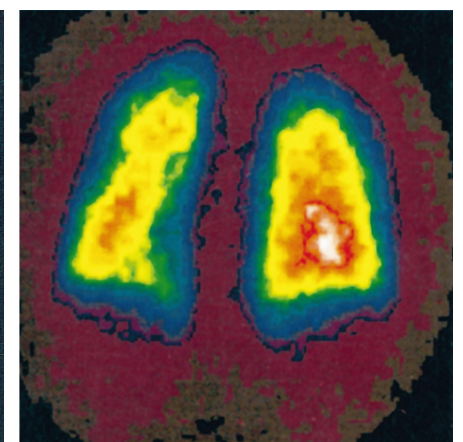

D

E

Fig 3. Patient 22: glioblastoma multiforme.

A, Sagittal contrast-enhanced T1-weighted MR image shows peripheral enhancement, possibly necrotic center, and perifocal edema, consistent with a glioblastoma multiforme (World Health Organization grade IV).

B, Right internal carotid angiogram shows typical aspect of glioblastoma multiforme: intense irregular parenchymal blush, formation of dilated abnormal intratumoral vessels (*long arrows*), and early venous drainage, in this case directed toward the superior longitudinal sinus and the cavernous sinus (*short arrows*).

C, Angiogram of a branch of the middle cerebral artery supplying the glioblastoma. The tip of the Tracker 10 microcatheter (*long arrow*) is situated in the arteria praefrontalis. The tumor is selectively blushing and the draining veins are already visible (*short arrows*). From this catheter position, ^{99m}Tc-MAA angioscintigraphy was performed.

D and *E*, Scintigrams of the head (*D*) and lungs (*E*) show intense pulmonary activity as a consequence of the intralesional shunt.

early appearance of draining veins is the result of decreased local cerebrovascular resistance. This may be due to direct communication between arteries and veins or to the presence of enlarged abnormal and/or dilated normal capillaries (15–17). The width of the capillary bed is influenced by the local metabolism; that is, an increased concentration of CO_2 and a low pH can generate luxury perfusion as a consequence of cerebrovascular occlusive lesions (18).

Even with the use of magnification angiography, only blood vessels with diameters as small as 200 μm can be seen directly. Arteriovenous shunts of this or an even larger diameter are often present in AVMs, but they are rare in tumors. With conventional angiography, it is not always possible to define the precise location and size of those large AVFs inside an AVM. Even with superselective catheterization of the

single feeder supplying the fistulous compartment of the AVM in combination with magnification and rapid serial digital angiography, it may be difficult to decide whether there is only one large direct or many smaller connections between the artery and draining vein, owing to the high velocity of the blood flow and the immediate opacification of the usually enlarged draining vein.

On the other hand, localized slowing of circulation with delayed emptying of arteries and late filling of veins may be the result of locally increased pressure caused by the space-occupying process itself and the surrounding edema or by restriction of the outflow in the draining veins, as observed in dural high-pressure, low-flow fistulas. This is, therefore, also compatible with the presence of arteriovenous shunts.

Although there is a great deal of histopathologic and electron microscopic data available
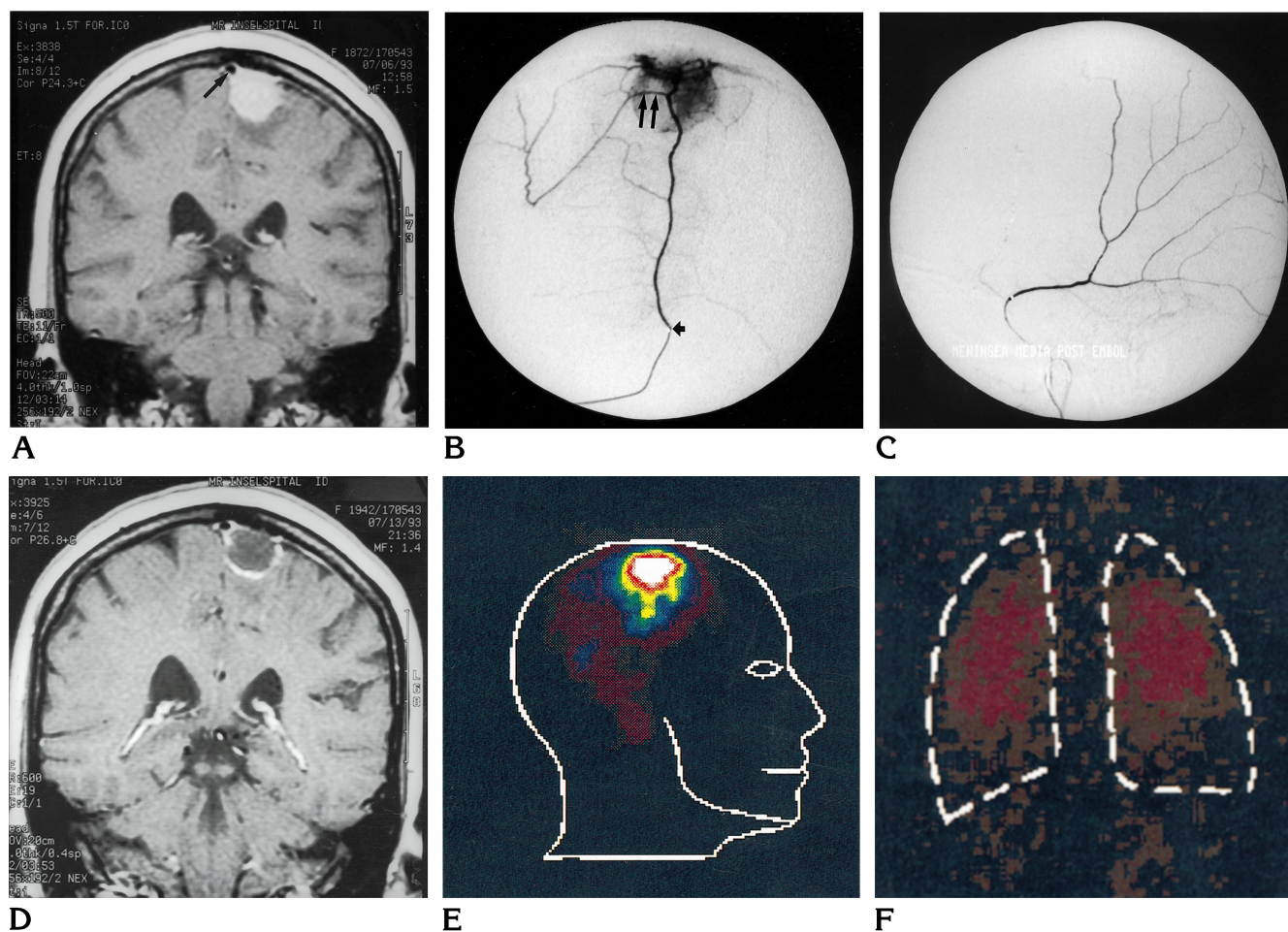
Fig 4. Patient 28: parasagittal meningioma.

A, Frontal contrast-enhanced T1-weighted MR image shows strongly enhancing left parasagittal meningioma attached in the region of the sinus longitudinalis superior (*arrow*), which is still patent.

B, Angiogram of a dorsal branch of the middle meningeal artery supplying the meningioma. From this catheter position (*short arrow*), a peritumoral anastomosis becomes visible (*long arrows*), probably due to the injection pressure.

C, Angiogram of the dorsal branch of the middle meningeal artery after embolization with particles of diameter 45 to 150 μm.

D, Frontal contrast-enhanced T1-weighted MR image 5 days after embolization. The disappearance of the central contrast enhancement signifies devascularization. Some contrast enhancement is still visible in the tumor capsule.

E and *F*, Scintigrams of the head (*E*) and lungs (*F*) show very high activity in the tumor region, and only background activity in the lungs. This finding was consistent with a PSI of 0%.

on tumors and vascular malformations, only some is helpful in predicting the extent and size of vascular anastomoses leading to arteriovenous shunting.

Brain scintigraphy with ^{131}I-MAA was used mainly as a diagnostic tool for brain tumors before the CT era (19–26). With intracarotid injection of ^{131}I-MAA, Handa et al (27) could estimate the global rate of short-circuited arterial blood. Picard et al (28) embolized 45 extracerebral craniospinal lesions using gelatin sponges marked with iodine-131. The next day, they controlled scintigraphically the embolized area and the thoracoabdominal region. These authors focused mainly on the distribution of the embolization material and they identified three patterns of tumor embolization: centrotumoral, peritumoral, and extratumoral, depending on the selectivity achieved by the catheterization of the vascular pedicles. They did not notice any scintigraphic activity on the thoracoabdominal region in any of the cases. This finding is not surprising if we consider the dry size of the gelatin pieces they used, the smallest measuring approximately $0.5 \times 0.6 \times 0.8$ mm. Conroy et al (29) used the same technique to embolize

Fig 5. Logarithmic scale shows the positive correlation between increasing TSR, as calculated with the hand-held detector in the angiography suite, and percentage of decreasing PSI, as calculated from gamma camera scintigraphy after embolization.
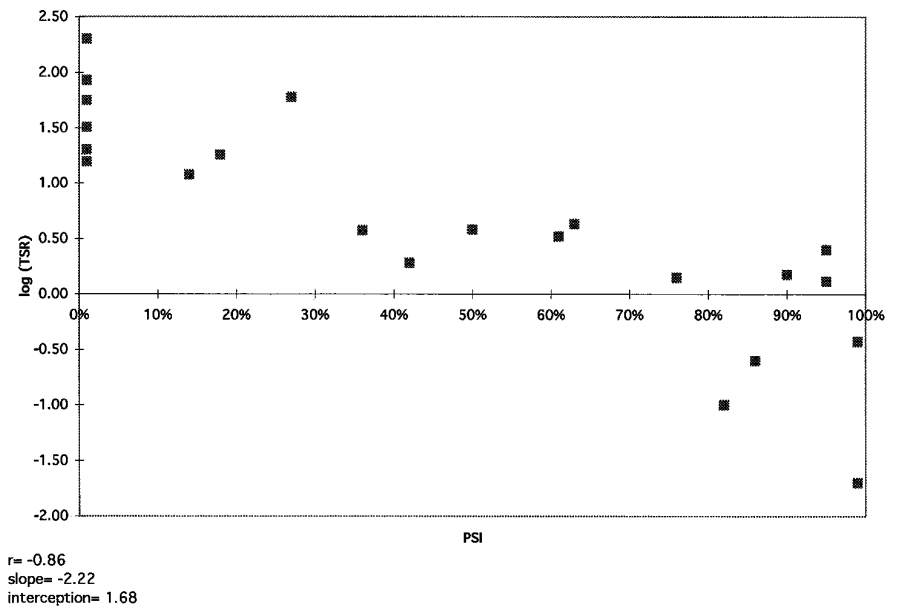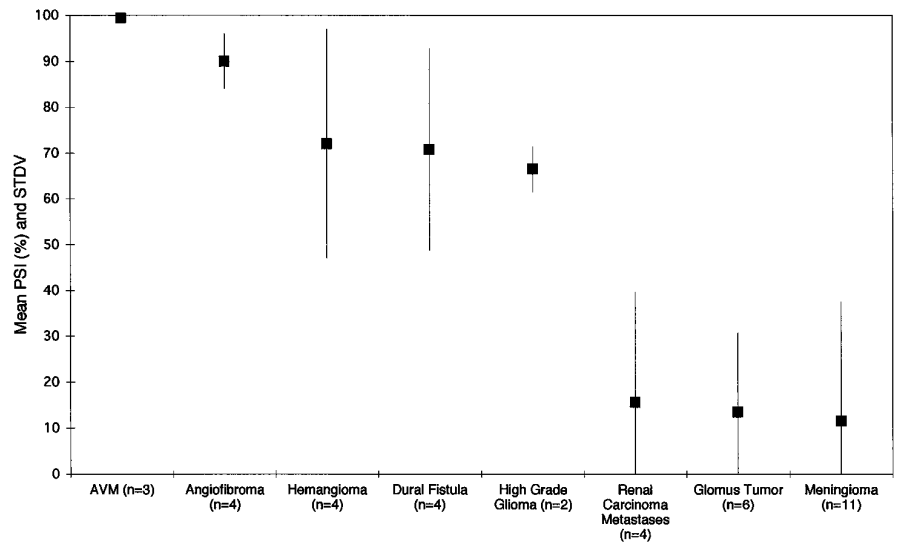

r= -0.86
slope= -2.22
interception= 1.68

Fig 6. Comparison of mean PSI values (±SD) for each histopathologic subgroup.

visceral lesions with gelatin sponges marked with technetium-99m. Reflux of this material to the thigh was documented in one case of transarterial embolization of the spleen. Translesional embolization to the lungs was documented in two cases during transvenous treatment of esophageal varices. Using the same embolization agent, Seo et al (30) documented translesional passage to the lungs in one case of dural AVF and no translesional shunting in a hemangioma of the back.

Each of the studies just described is limited by the relatively large size of the catheters used, and thus the reduced selectivity; by a lack of information concerning the real size of the em-

bolic material; and by a lack of quantification of the amount of translesional shunting.

Jack et al (31) refined the method by labeling PVA microparticles (average size, about 0.5 mm) with technetium-99m, and demonstrated complex stability and biodistribution after intravenous and intracarotid injection in animals. These investigators documented the location of the embolic material in and around a large pteryonal meningioma after injection in the distal external carotid artery. In one case of an AVM of the thigh, Sirr et al (32), using a mobile gamma camera installed in the angiographic suite, documented reflux and distal migration of large ^{99m}Tc-marked PVA particles in the calf

but no translesional arteriovenous shunting to the lungs. In one case of a pelvic AVM, migration to the lungs was identified during the procedure, prompting the researchers to modify the position of the catheter to avoid this pulmonary shunting.

To optimize intraarterial chemotherapy of cervicofacial malignancies, Wheeler et al (10) injected ^{99m}Tc-MAA into the external carotid artery of nine patients. These authors calculated a mean systemic shunt of 23% (range, 11% to 44%), a mean tumor blood flow of 13.6 mL/100 mg per minute, and a ratio of tumor/normal tissue blood flow of 5.6 using a xenon-133 washout technique.

Using microcatheter techniques, we injected ^{99m}Tc-MAA particles with a diameter of 25 to 50 μm superselectively into small arteries, which exclusively supplied different cerebrospinal lesions in 38 patients. With this technique, it was possible to see the extension and distribution of the embolic material inside the lesion as well as to measure the pulmonary trapping of the ^{99m}Tc-MAA particles that shunted through the arteriocapillary bed of the lesions.

We tested the reliability of a portable detector as compared with measurements made with the use of a gamma camera. The positive point about this hand-held system is its practicality: it is easy to handle and not time-consuming, and it allows focused application on the region of interest and rapid calculation of a selectivity ratio. A TSR of more than 10 was always associated with a PSI of less than 30% (see "Results"). However, we used very small microparticles (45 to 150 μm) only in those instances in which almost no activity was detected over the lungs. The major limitation of this portable detector is that the recording depends on how the probe is held over the region of interest, which makes the measurement somewhat examiner-dependent. However, an estimation of whether an important pulmonary shunt exists or not is always possible. In contrast, a precise TSR cannot be calculated in every case. The use of a movable gamma camera in the angiography suite could overcome these limitations but would probably prolong the procedure.

Performing scintigraphy of tumor and lung with a gamma camera after definite embolization allowed us good visual representation and quantification of microparticle shunting to the lungs. As expected, a high, almost complete pulmonary shunting was seen in AVMs, demonstrating the presence of arteriovenous communications clearly larger than 25 μm. This was also evident in the patient with exclusively plexiform angioarchitecture (case 2). Angiographically, this was already suspected in most of these lesions on the basis of the appearance of large fistulas and because of the very rapid circulation time with appearance of draining veins during the early arterial phase. Despite the presence of similar visible arteriovenous channels, the PSI was not as high in dural fistulas.

Hemangioblastomas are composed of a fine mesh of blood spaces and capillary channels that may be seen dilated into large sinuses (33–35). In our study, this tumor showed the typical intense parenchymal blush and the rapid appearance of contrast medium in draining veins. A similar angioarchitecture was also found by intraarterial DSA in a capillary venous angioma and in an AVM of the face. We identified an important arteriovenous shunt in both.

Vertebral hemangiomas are usually of the cavernous type and show a slow circulation time at angiography, sometimes with contrast medium stagnating in the tumor and draining veins (17). Despite these angiographic characteristics, we found a significant intralesional shunt in one patient (PSI = 42%). As we recently reported in a smaller series (36), we found a surprisingly low PSI in paragangliomas. Willis and Birrell (37) made an in-depth study of the microvasculature of a paraganglioma of the carotid body with special emphasis on the unique anastomosing pattern in this tumor type. Even if large cavernous and hypertrophic vessels were found in this tumor, no direct communication between arteries and veins exceeding a caliber of 13 μm was described in their article. Accordingly, our data suggest that potentially no or a low arteriovenous shunt results from injection of particles as small as 25 μm in diameter, which seems to be a promising result, considering the possible future options of microspheric radioembolization or chemoembolization of this type of tumor. In contrast, a very high PSI was observed in the four patients with juvenile angiofibroma, despite the angiographic similarity between this tumor and paragangliomas.

Glioblastomas have angiographically typical areas of vascular shunts, with a relatively high flow and a vascular bed of moderate size. In arteriography, the contrast medium thus appears early and is washed out early, usually

simultaneously with the appearance of the draining veins, as in our patient with this type of tumor. Our findings in this patient support the hypothesis of an important arteriovenous anastomosis component in these tumors. The same finding characterized one anaplastic oligodendroglioma, which had the same angiographic pattern as glioblastoma. Because of this important arteriovenous shunting, no significantly better potential for cell killing or lower systemic toxicity can be expected after intraarterial chemotherapy in these malignant gliomas as compared with systemic intravenous application. Experimental approaches using chemotherapeutics encased in microspheres (38, 39) might better reach those goals.

In metastases of renal cell carcinoma, we observed 0% to 50% PSI. Two such tumors showed a rapid circulation time with an early appearance of veins; however, in neither tumor was an intralesional shunt detected with our method. We found very low shunt rates in meningiomas, less than 5% in nine of 11 tumors. Interestingly, four of these tumors had evidence of early venous drainage, but in only two of them was a significant intralesional shunt detected. These data suggest that particles as small as 25 μm could be used to optimize presurgical embolization in most meningiomas (Fig 4).

In summary, our method identified three groups of lesions according to the amount of intralesional arteriovenous shunting: those with high PSI, including AVMs and angiofibromas; those with medium-high PSI, including hemangiomas, dural fistulas, and high-grade gliomas; and those with low PSI, including meningiomas, glomus tumors, and renal cell carcinoma metastases. The size of our subgroups was too small to permit general conclusions for every tumor type.

The presence of visible arteriovenous channels at angiography was associated with a high intralesional microparticle shunting; however, a rapid circulation time as assessed by the presence of early venous drainage at angiography was not a good predictor of intralesional microparticle shunting in paragangliomas, renal cell carcinoma metastases, and meningiomas. The early venous drainage in these tumors was probably due to the presence of a widespread network of dilated capillaries that were smaller than the particles used.

Conclusion

Superselective angioscintigraphy with ^{99m}Tc-MAA allows quantification of the intralesional arteriovenous shunting of microparticles with a caliber of 25 to 50 μm in tumors and vascular malformations of the head and spine, including those in the central nervous system. The amount of microparticle shunting in tumors seems to be related to the histopathologic diagnosis and to some angiographic characteristics but not to the size of the lesion. Superselective angioscintigraphy and on-line measurement of the pulmonary shunt rate in the angiography suite can be useful complementary tools for determining the ideal size of embolic agents for a given lesion.

References

1. Lasjaunias P, Berenstein E. *Surgical Neuroangiography, II: Endovascular Treatment of Craniofacial Lesions.* Berlin, Germany: Springer; 1987:101–162
2. Valavanis A. *Interventional Neuroradiology.* Berlin, Germany: Springer; 1993:77–92
3. Vinuela F, ed. *Interventional Neuroradiology: Endovascular Therapy of the Central Nervous System.* New York, NY: Raven Press; 1992:24–28
4. Laurent A, Beaujeux R, Wassef M, Ruefenacht D, Boschetti E, Merland JJ. Trisacryl gelatin microspheres for therapeutic embolization, I: development and in vitro evaluation. *AJNR Am J Neuroradiol* 1996;17:533–540
5. Beaujeux R, Laurent A, Wassef M, et al. Trisacryl gelatin microspheres for therapeutic embolization, II: preliminary clinical evaluation in tumors and arteriovenous malformations. *AJNR Am J Neuroradiol* 1996;17:541–548
6. Kato T, Nemoto R, Mori H, et al. Arterial chemoembolization with microencapsulated anticancer drug. *JAMA* 1981;245:1123–1127
7. Kato T, Nemoto R, Mori H, Takahashi M, Tamakawa Y. Transcatheter arterial chemoembolization of renal cell carcinoma with microencapsulated mitomycin C. *J Urol* 1981;125:19–24
8. Okamoto Y, Konno A, Togawa K, Kato T, Amano Y. Microcapsule chemoembolization for head and neck cancer. *Arch Otorhinolaryngol* 1985;242:105–111
9. Leung W, Lau W, Ho KL, et al. Measuring lung shunting in hepatocellular carcinoma with intrahepatic arterial technetium 99m macroaggregated albumin. *J Nucl Med* 1994;35:70–73
10. Wheeler RH, Ziessman HA, Medvec BR, et al. Tumor blood flow and systemic shunting in patients receiving intraarterial chemotherapy for head and neck cancer. *Cancer Res* 1986;46:4200–4204
11. Walser RH, Haldemann AR, Rösler H, Koranda P, Kinser JA, Triller J. Diagnostic angioscintigraphic evaluation of malignant hepatic tumors before catheter embolization: determination of shunt, flow distribution and reflux. *Cardiovasc Intervent Radiol* 1996;19:77–81
12. Nomura F, Ohnishi K, Terabayashi H, et al. Effect of intrahepatic portal systemic shunting of hepatic ammonia extraction in patients with cirrhosis. *Hepatology* 1994;20:1478–1481

13. Clarke SEM, Secker-Walker RH. Lung scanning. In: Maisey MN, Britton KE, Gilday DL, eds. *Clinical Nuclear Medicine.* 2nd ed. London, England: Chapman & Hall Medical; 1991:47–74

14. Lau WY, Leung WT, Leung NW, et al. Treatment of inoperable hepatocellular carcinoma with intrahepatic arterial yttrium-90 microspheres: a phase I and II study. *Br J Cancer* 1994;70:994–999

15. Greitz T. A radiologic study of the brain circulation by rapid serial angiography of the carotid artery. *Acta Radiol* 1956; suppl 140

16. Greitz T. Evaluation of the circulation time in angiography of the vertebral artery. *Acta Radiol* 1969;9:300–309

17. Newton TH, Potts DG. *Radiology of the Skull and Brain: Angiography.* St Louis, Mo: Mosby; 1974:2:book 1:1049–1088

18. Lassen LA. The luxury perfusion syndrome and its possible relation to acute metabolic acidosis localised within the brain. *Lancet* 1966;2:1113–1115

19. Kennady JC, Taplin GV. Albumin macroaggregates for brain scanning: experimental basis and safety in primates. *J Nucl Med* 1965;6:566–581

20. Rosenthall L. Human brain scanning with radioiodinated macroaggregates of human serum albumin. *Radiology* 1966;85:110–115

21. Rosenthall L, Augayo A, Stratford J. Clinical assessment of carotid and vertebral artery injection of macroaggregates of radio-iodinated albumin (MARIA) for brain scanning. *Radiology* 1966;86:499–505

22. Kaneko M, Sasaki T, Kido C. Positive scintigraphy of tumor by means of intra-arterial injection of radio-iodinated macroaggregated albumin (MAA). *AJR Am J Roentgenol* 1968;102:81–87

23. Murphy SE, Cervantes RC, Maass ER. Radioalbumin macroaggregate brain scanning: a histopathologic investigation. *AJR Am J Roentgenol* 1968;102:88–92

24. Armenise B, Conforti P, Blandino G, Bonanno N. Der Wert der Hirnszintigraphie mit MAA-J131 bei intraarterieller Injektion in die Arteria carotis. *Acta Neurochir* 1968;19:139–148

25. Huber P, Rösler H. Die Bedeutung der Angioszintigraphie in der Neuroradiologie. *Schweiz Med Wochenschr* 1969;99:757–763

26. Briz-Kanafani S, Constantino GL. Perfusion I131-macroaggregate brain scanning: a clinical evaluation or its diagnostic efficiency. *AJR Am J Roentgenol* 1968;109:686–691

27. Handa J, Iwayama K, Yonekawa Y, Yoshida Y, Handa H. The use of MAA-I131 in cerebral arteriovenous fistulas. *AJR Am J Roentgenol* 1968;104:18–28

28. Picard L, Robert J, André JM, et al. Embolisation of Spongel marqué à l'iode 131: technique, indications et résultats. *J Neuroradiol* 1976;3:53–74

29. Conroy RM, Lyons KP, Kuperus JH, Juler GL, Joy I, Pribram HFW. New technique for localization of therapeutic emboli using radionuclide labeling. *AJR Am J Roentgenol* 1978;130:523–528

30. Seo JS, Furui S, Kokubo T, et al. Embolism detection and prevention using scintigraphy during therapeutic arterial blockade. *Radiology* 1985;157:815–816

31. Jack CR, Dewanjee MK, Brown ML, Forbes G, Chowdury S. Radiolabeled polyvinyl alcohol particles: a potential agent to monitor embolization procedures. *Int J Radiat Appl Instrument (Part B: Nucl Med Biol)* 1986;13:235–243

32. Sirr SA, Johnson TK, Stuart DD, et al. An improved radiolabeling technique of Ivalon and its use for dynamic monitoring of complications during therapeutic transcatheter embolization. *J Nucl Med* 1989;30:1399–1404

33. Russel DS, Rubinstein LJ. *Pathology of Tumours of the Nervous System.* 5th ed. London, England: Arnold; 1989:639–663

34. Ho KL. Ultrastructure of cerebellar capillary haemangioblastoma: mast cells and angiogenesis. *Acta Neuropathol* 1984;64:308

35. Ho KL. Ultrastructure of cerebellar capillary haemangioblastoma: pericytes and their relationships to endothelial cells. *Acta Neuropathol* 1985;67:254

36. Schroth G, Haldemann A, Mariani L, Remonda L, Raveh J. Preoperative embolization of paragangliomas and angiofibromas: measurement of intratumoral arterio-venous shunts. *Arch Otolaryngol Head Neck Surg* 1996;122:1320–1325

37. Willis AG, Birrell JHW. The structure of a carotid body tumor. *Acta Anat* 1955;25:220–265

38. Fujimoto S, Endoh F, Kitsukawa Y, et al. Continued in vitro and in vivo release of an antitumor drug from albumin microspheres. *Experientia* 1983;39:913–916

39. Yang J, Ma X, Zou Z, Wei S. Experimental maxillofacial arterial chemoembolization with encased cisplatin ethylcellulose microspheres. *AJNR Am J Neuroradiol* 1995;16:1037–1041